Geophysical Journal International

Geophys. J. Int. (2020) **224,** 207–215
Advance Access publication 2020 September 22
GJI Seismology

doi: 10.1093/gji/ggaa447

Seismic noise monitoring of a small rock block collapse test

Marco Taruselli,[1] Diego Arosio,[2] Laura Longoni,[1] Monica Papini[1] and Luigi Zanzi[1]

[1] *Politecnico di Milano, Dipartimento di Ingegneria Civile e Ambientale, Piazza L. Da Vinci* 32, 20133 *Milano, Italy*
[2] *Dipartimento di Scienze Chimiche e Geologiche, Università degli Studi di Modena e Reggio Emilia, Via G. Campi* 103, 41125 *Modena, Italy.*
E-mail: diego.arosio@unimore.it

Accepted 2020 September 18. Received 2020 September 11; in original form 2020 January 10

SUMMARY

We tested the capability of seismic noise to monitor the stability conditions of a small rock block that we forced to fail in four following stages. Ambient vibrations were recorded with a broad-band 3C seismometer placed on top of the block and were processed to analyse their spectral and polarization characteristics with diverse algorithms. To analyse the spectral content of the records, we applied the multitaper method while seismic noise polarization features were investigated by means of the singular value decomposition of the Hermitian spectral density matrix. Numerical modelling was found to add limited value because of the uncertainty in estimating correctly spatial and mechanical features of the rock bridges between the block and the rock mass. Nevertheless, a modelling exercise we performed is in agreement with previous post-failure observations according to which unstable rocks may be coupled to the stable rock mass by rock bridges covering only a few per cent of the total surface of the fractures. Our analyses confirm that, when approaching final collapse, there is a trend of the block eigenmodes towards lower frequencies and show that polarized bands become narrower.

Key words: Fourier analysis; Instability analysis; Numerical modelling; Time-series analysis; Seismic instruments; Seismic noise.

1 INTRODUCTION

Whenever excited, a rock structure can vibrate at its peculiar resonance frequencies associated with its different vibration modes. The resonance frequencies are dependent upon the geometry, the elastic constants, the density and the characteristics of the constraints of the studied rock structure (Bottelin *et al.* 2017; Burjánek *et al.* 2019). In addition, meteorological parameters can alter the vibration frequencies by means of both reversible and irreversible effects, as several authors observed correlation between resonance frequency and temperature, rainfall as well as wind (Levy *et al.* 2010; Bottelin *et al.* 2013b, 2017; Starr *et al.* 2015; Colombero *et al.* 2017; Valentin *et al.* 2017).

Seismic noise recording sessions can be effectively performed for monitoring purposes, according to the fact that a drop in natural frequencies has been observed as an unstable rock compartment approaches failure, because of reduced constraints and increased mass (Bottelin *et al.* 2013a, 2017; Valentin *et al.* 2017). Clear evidence of this phenomenon has been also observed in the civil engineering field, with buildings that show a drop in their vibration modes as a result of stiffness decrease due to earthquake damages (Potenza *et al.* 2015; Saisi *et al.* 2015; Lorenzoni *et al.* 2018). Moreover, higher spectral amplitudes are generally observed on the unstable body compared to the stable rock mass (Bottelin *et al.* 2017; Arosio *et al.* 2018). The approaches proposed in the scientific literature involve that collected ambient vibration data are processed to study their spectral and polarization features as a function of time (Burjánek *et al.* 2018). In more detail, frequency peaks and preferential directions of motion corresponding to vibration modes are sought for by considering periodograms and spectrograms, and different processing algorithms are applied in both time and frequency domains to estimate polarization in the 3-D space (Arosio *et al.* 2019b). Since several authors have investigated column-like rock structures partially detached from the rock mass, a standard analysis consists in estimating the horizontal-to-vertical spectral ratio (HVSR) and the HVSR as a function of azimuth (HVSRA). Recent applications of ambient vibration monitoring to rock structures have addressed more complex geometries like rock arches (Starr *et al.* 2015), the monitoring of bolting works applied to unstable rock columns (Bottelin *et al.* 2017), as well as the capability of the technique to detect the presence of more than one major discontinuity between the rock mass and the prone-to-fall rock compartment (Valentin *et al.* 2017). Seismic noise monitoring has been also successfully applied to slopes prone to sliding to study amplification and directional effects, especially in terms of site response to earthquakes (Del Gaudio & Wasowski 2007; Moore *et al.* 2011; Burjánek *et al.* 2012). Improvements concerning seismic noise studies on unstable rock structures could be borrowed to monitor: (i) drops in natural frequency of buildings as a result of stiffness decrease due to earthquake damages (Clinton *et al.* 2006); (ii) the effectiveness of

rock bolting works (Bottelin *et al.* 2017) and (iii) preferential polarization on sliding rock slopes and its relationship with measured displacements (Burjánek *et al.* 2012).

In this work. we analyse seismic noise data collected during a field test in which a rock block was forced to collapse. Though relatively small, the investigated block has an irregular geometry defined by one rear and one side fracture and it is different from the column-like geometry of rock structures usually investigated in the scientific literature. We consider both spectral and polarization analyses, the support of numerical modelling, with the final aim of identifying particular features of the collected seismic noise that might be used for rock failure forecasting purposes.

2 FIELD TEST

The controlled collapse test was performed in 2018 January on an unstable rock block located in the lower section of a 200-m high cliff diving into Como Lake, in the Italian Prealps (Fig. 1a). The slope consists entirely of *Perledo-Varenna* limestone having subhorizontal bedding (S0, 8/16) with thickness ranging from 0.1 to 1 m. In addition, the geological and photogrammetric surveys identified two main joint families approximately perpendicular to each other, namely K1 (245/85) and K2 (155/86), that may promote both plane and wedge failures. The unstable rock compartment selected for the experiment had an approximately trapezoidal prism shape of $0.7 \times 0.7 \times 0.3$ m $L \times H \times W$, resulting in a total volume of about 0.15 m^3 (Fig. 1b). From a structural point of view, the rock block was partially detached from the rock mass by two main fractures, namely F1 and F2 belonging to K1 and K2 joint sets respectively, and it was delimited at top and at the bottom by the bedding discontinuities (Fig. 1b). Actually, the block was divided into two parts, with a top bigger one laying onto a smaller one (Fig. 1b), that fell together when ultimate collapse occurred at the end of the test and split apart after the impact onto the ground (Fig. 1d).

To record ambient noise, we installed a *Nanometrics Trillium Compact* 20 s seismometer on top of the unstable block with the *Z* and *Y* components oriented along the vertical and the north–south directions, respectively (Fig. 1b). The sensor was coupled to a Nanometrics Centaur data logger and we set a sampling frequency of 1000 Hz. The sampling frequency has been defined by performing eigenfrequency analysis tests with *COMSOL Multiphysics* software on cubic-shaped blocks modelled with the same volume and geomechanical properties of the studied rock block. We performed the modal analysis testing different areas for the rock bridges to have an insight of the resonant frequencies of the real case study and found out that a sampling frequency of 1000 Hz was sufficient to record roughly the first six vibration modes of the unstable rock block. Though generally recommended, we could not deploy any reference station on the rock mass to effectively isolate the response of the monitored rock block mainly because of the impossibility to safely reach the top of the 200-m high cliff and to find a position on the cliff face whose vibrations could be confidently interpreted as representative of the whole rock mass behaviour. During the test, fracture F2 was mechanically widened with an iron lever approximately every 30 min and four stages were performed before ultimate collapse. Fracture F2 was chosen because of its higher initial persistence and aperture with respect to F1. Ambient vibrations have been continuously recorded and, at the beginning of each stage, sensor levelling was checked and fixed whenever necessary to be sure noise was constantly collected along the same directions, and the fracture aperture was measured in four distinct control points along F2 using a digital calliper (Fig. S1, Supporting Information). Collected ambient vibrations have been divided into five subsignals according to the different stages of the test, with stages 0 and 4 corresponding to the initial undisturbed condition and to the condition immediately before ultimate failure, respectively. Before performing spectral and polarization analyses, the time-series recorded during each stage has been time-cut to discard the first 10 min in order to remove transients caused by fracture widening and to take into account sensor stabilization after re-levelling. Subsequently, time-series have been deconvolved to remove the instrument response (Templeton 2017) and filtered with a zero-phase 0.5 Hz high-pass filter to attenuate low-frequency components greatly amplified by the deconvolution process.

In order to study variations of rock block vibration in response to climatic parameters, we took into account data collected by meteorological stations located close to the lake shore approximately 4 and 5.5 km south of the test site (Fig. S2, Supporting Information).

3 DESCRIPTION OF METHODS

3.1 PSD estimation

We studied the spectral content of the collected seismic noise by estimating the power spectral density (PSD) by means of a non-parametric spectral estimation method, namely the multitaper method (MT) first proposed by Thomson (1982). Like other spectral estimation techniques, the MT method is aimed to reduce bias and variability of the PSD estimate. Bias is reduced thanks to the use of tapers taken as a set of mutually orthogonal functions that are chosen to have optimal time–frequency concentration properties. Variability is reduced by averaging over approximately uncorrelated PSD estimates that are obtained through orthogonal tapers (Percival & Walden 1993). To perform the computations, we set a frequency resolution W of 1 Hz and a number of tapers equal to $2TW$-1 (Percival & Walden 1993), where T is the signal duration in seconds, that is, the duration of each stage in our case. Conversely to what is commonly done in seismic site resonance analysis (e.g. Konno & Ohmachi 1998), we did not apply any additional spectral smoothing so as to avoid any merging of close spectral peaks possibly related to different vibration modes of the studied structure (Arosio *et al.* 2019a).

3.2 Polarization analysis

We performed a polarization analysis to study preferential oscillation directions associated to the eigenmodes of the rock block during the different stages of the collapse test. We took into account the singular value decomposition (SVD) of the Hermitian spectral density matrix (Samson 1983). Considering the general case of elliptical particle motion in the 3-D space, the spectral SVD approach can provide a complete set of polarization features overcoming the drawbacks of other methodologies (Arosio *et al.* 2019b). As a matter of fact, spectral SVD allows to perform the analysis as a function of frequency, in the 3-D space and to estimate the phase lags between the components of the polarization vector. To quantify polarization, we compute the degree of polarization parameter β^2 from the matrix of the singular values (Samson 1983). β^2 can range from 0 to 1, the former corresponding to unpolarized signals and the latter indicating a well-defined polarization; high values of β^2 do not necessarily imply linear polarization, as circular or elliptical particle motion

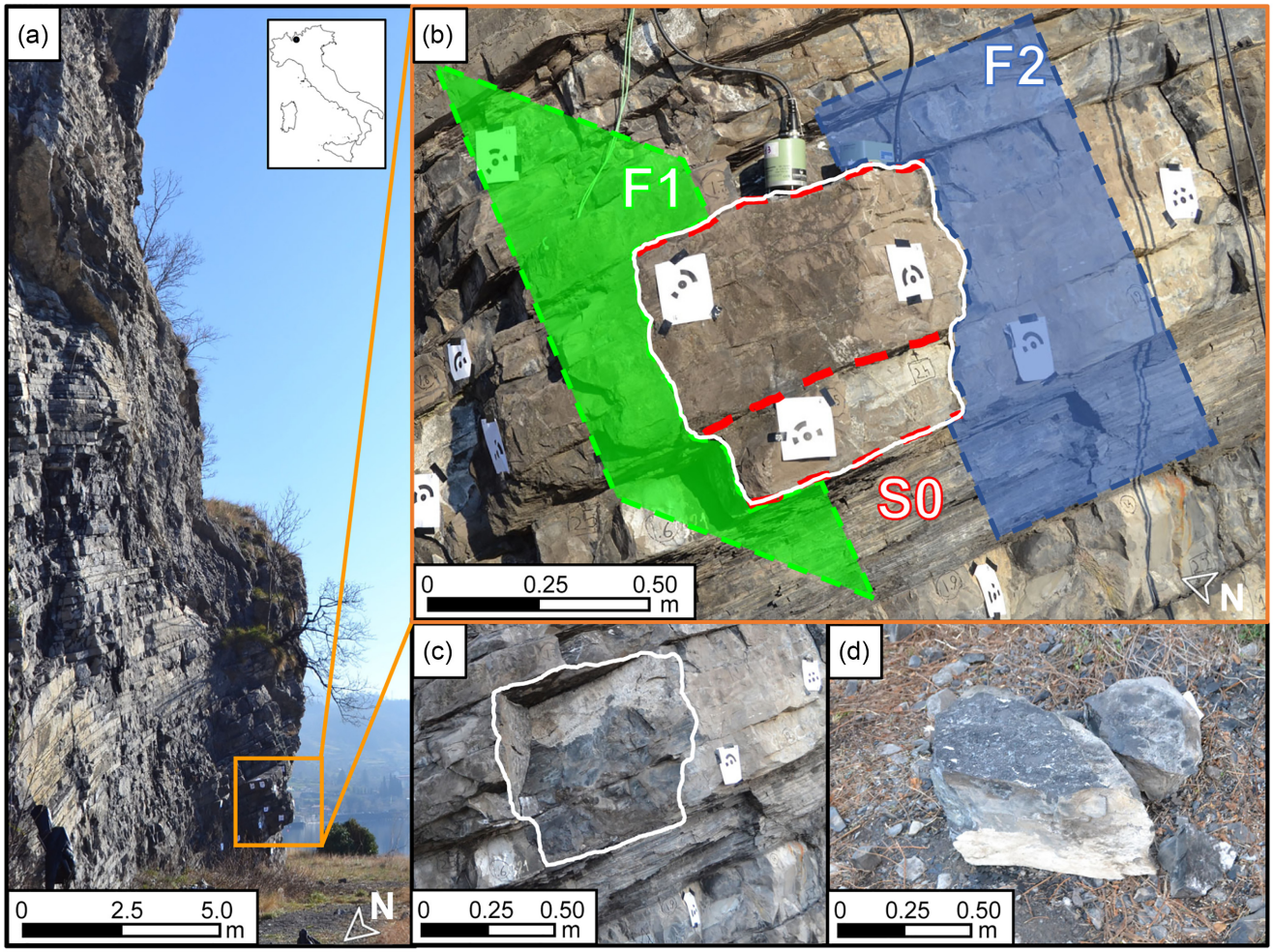

Figure 1. Pictures taken at the site where the test was performed. (a) Rock cliff. (b) The rock block that was forced to collapse (white contour) with the two main fractures F1 and F2 together with the bedding S0 (targets for the photogrammetric survey are also visible); Nanometrics Trillium Compact sensor is placed on top of the block. (c) Pictures of the rock surface after the failure and (d) of the collapsed blocks.

can provide high values as well. In addition, we estimate frequency-dependent angular quantities by projecting along the three axes the complex right eigenvector associated to the dominant (if any) singular value (Park *et al.* 1987). In more detail, Θ_H is the azimuth of the main polarization axis measured counterclockwise from east, Θ_V is its dip measured form the horizontal, while ϕ_{HH} and ϕ_{VH} indicate the phase relationships between the two orthogonal horizontal components and between the vertical and the principal horizontal components, respectively.

3.3 Numerical modelling

We performed an eigenmode analysis of the studied rock block with the finite-element software *COMSOL Multiphysics* to support the interpretation of the results obtained with the spectral and polarization analyses. Our aim was to investigate the relationship between the observed fundamental frequency drop and the rock-bridges breakage, and to simulate the block eigenmodes to confirm the polarization of seismic noise detected during the experimental test.

The unstable block has been modelled as an undamped system with multiple degrees of freedom. The 3-D geometry was built by meshing the point cloud obtained through the photogrammetric survey with tetrahedral finite elements. However, the back and side of the block were approximated with plane surfaces. The rock block has been considered as an isotropic, homogeneous medium with density 2680 kg m^{-3}, Poisson ratio 0.3 and Young's modulus 30E9 N m^{-2}. The latter parameter was estimated using an empirical equation relating Young's modulus and Schmidt hammer rebound values recorded in the field (Katz *et al.* 2000). In addition, the estimated values were crosschecked by using an empirical chart that relates Young's modulus to both density and the point load strength index (Sonmez *et al.* 2006) obtained by performing the point load test according to the International Society for Rock Mechanics guidelines (Franklin 1985).

We set the constraints of the block model at locations where fresh rock ruptures were thought to be observed after the collapse. In more detail, fracture F2 is characterized by an upper brighter section covered by a calcite layer, which denotes that the block was already partially detached from the cliff, and by a lower darker section that might show evidences of rock bridge breakage due to the collapse test (Fig. 1c). According to this, we tried to detect newly exposed rock areas by identifying groups of pixels with values ranging in a pre-determined interval in the Red-Green-Blue (RGB) matrix of nearly frontal images of fractures F1 and F2. Images were first smoothed with a 2-D convolutional filter to limit scattering of the identified points. The estimated rock bridges (Fig. 4a) were

then modelled with the same geomechanical properties of the rock mass. In particular, an elastic constraint has been introduced for each identified contact surface imposing an isotropic stiffness of 3E10 $\mathrm{N\,m^{-3}}$. The bedding interface between the two parts of the block (Fig. 1b) was modelled as an anisotropic elastic thin layer with normal (*kn*) and shear (*ks*) stiffness of 1.5E10 and 2.1E9 $\mathrm{N\,m^{-3}}$, respectively, in agreement with the values proposed for limestone by Kulatilake *et al.* (2016).

4 RESULTS

4.1 Seismic monitoring

The obtained PSD estimates reveal several spectral peaks at relatively high frequency, in the range 50–300 Hz, in agreement with the small size of the specimen (Fig. 2). To ease visual interpretation of the evolution of spectral peaks across following stages of the test, we also used the short-time Fourier transform (5 s signal subwindows, Hamming taper, 50 per cent overlap) to compute the spectrograms that are displayed together with the MT results in Fig. 2. We identified two main decreasing trends over time roughly associated to two different frequency bands. A first high-frequency peak moves from about 220 to 150 Hz and it is more easily interpreted on the vertical component. The second frequency peak is clearly observed along the east–west direction, appears to be the dominant peak (though may not be the fundamental) and shifts from around 150 Hz at the initial condition to 80 Hz prior to collapse. In more detail, the lower frequency peak actually involves several different peaks that split up and approach monochromatic signals towards failure. Finally, during the second and third stages of the test, we observe the occurrence of high-amplitude signals at frequencies below 10 Hz on the horizontal components only.

Given the complex geometry of the block (i.e. non-column-like) and of the constraints, the recorded seismic noise has a large vertical component, and peaks and troughs of both horizontal and vertical spectra interfere in a complex manner. Accordingly, the related HVSR curve would be extremely difficult to be interpreted. Therefore, we did not consider the HVSR method to process our data set.

Fig. 3 illustrates the polarization parameters estimated with the spectral SVD for the all the stages. Parameters were computed using 10 s Hamming-tapered time windows with 90 per cent overlap, and 20 spectral density matrices were averaged in the frequency domain (Koper & Hawley 2010). Results are presented in terms of relative probability, that is, for each frequency, the estimated values of the parameter are partitioned into bins and the value of each bin is the ratio of the number of elements in the bin to the total number of elements (i.e. the sum of all the bin values gives unity).

β^2 values close to 1 through the different test stages indicate that polarization is significant over several frequency bands between 50 and 300 Hz. The polarization parameters have higher probability values around 130–140 Hz during the first three stages, whereas higher probability values are observed around 65–75 Hz for the last two stages. In fact, the most dramatic change is from stages 2 to 3 and may correspond to the highest increase in the aperture of the solicited fracture (Fig. S1, Supporting Information). Because of the oscillating nature of the vibration modes, it is meaningful to display Θ_H probability values just over a 180°-wide interval. For the first three stages, the maximum probability values cluster around 0°, revealing that, actually, there is some minor displacement along the east–west direction perpendicular to fracture F1, even at the initial stage. This finding is supported by the non-zero values of ϕ_{HH} clusters, that progressively decreases from −20° to −70° until stage 2, indicating that the polarization in the azimuthal plane is elliptical. Higher probability values for Θ_V generally cluster close to 0°, hence the dominant vibration mode has negligible vertical motion, although the block does exhibit at least one higher frequency mode with significant vertical displacement. ϕ_{VH} probability values are lower than the values of the other parameters because the azimuthal displacement of the dominant mode and the vertical displacement of the higher mode dwarf their respective vertical and horizontal displacements.

4.2 Numerical modelling

The block behaviour modelled according to its estimated mechanical parameters and to the estimated mechanical and geometrical features of the rock bridges gave results showing unsatisfactory matching with real data in terms of both resonance frequency and polarization. In fact, we obtained poor outcomes at all the stages of the test, that were modelled by assuming a gradual reduction of rock bridges caused by a progressive opening of the rear fracture F2 (Fig. 1b), starting from where the destabilizing force was applied. We did observe a gradual shift of the eigenmodes towards lower frequencies, but neither the spectral peaks nor the modal shapes matched the measured ones (Fig. 4b).

Given the poor obtained results, as a modelling exercise, we discretized the side and rear surfaces of the rock block (excluding the calcite area) and ran several simulations tuning the geometrical configurations of the rock bridges and the bedding stiffness values in order to match the first five resonance frequencies observed during stages 0 and 4. Final normal and shear stiffness values for the bedding, respectively 3E10 and 9E9 $\mathrm{N\,m^{-3}}$, are in good agreement with the ones proposed by Kulatilake *et al.* (2016) for limestone. Figs 4(c)–(f) show the best models with an average mismatch between observed and modelled resonance frequencies lower than 5 per cent (Table 1).

5 DISCUSSION

In this study, we processed seismic noise recordings collected with a 3C broad-band velocimeter deployed on top of a 0.15 $\mathrm{m^3}$ limestone block that was forced to collapse through four following stages. To fully test the effectiveness of the technique, we decided to select a rock structure with arbitrary geometry, though not too complex, being separated from the rock mass by rear and side fractures and possibly having similar moments of inertia about orthogonal axes. This is different from case studies investigated in the scientific literature, that generally consider bigger isolated rock columns with a single rear fracture and thus could approximate slender beams with preferential oscillation in the azimuthal plane perpendicular to the rear fracture plane (Bottelin *et al.* 2013a; Valentin *et al.* 2017).

The spectral analysis we performed confirms that there is a decreasing trend of resonance frequencies towards failure (Levy *et al.* 2010). It is clear that vibration modes varied dynamically across the test, according to changes occurred to the constraints between the block and the rock mass. Some frequency peaks are only visible on a single component (Fig. 2), suggesting the polarization of the associated modes. The presence of several closely spaced and transient frequency peaks prevents a quantitative estimate of the decrease through the stages, but considering the two main vibration modes in

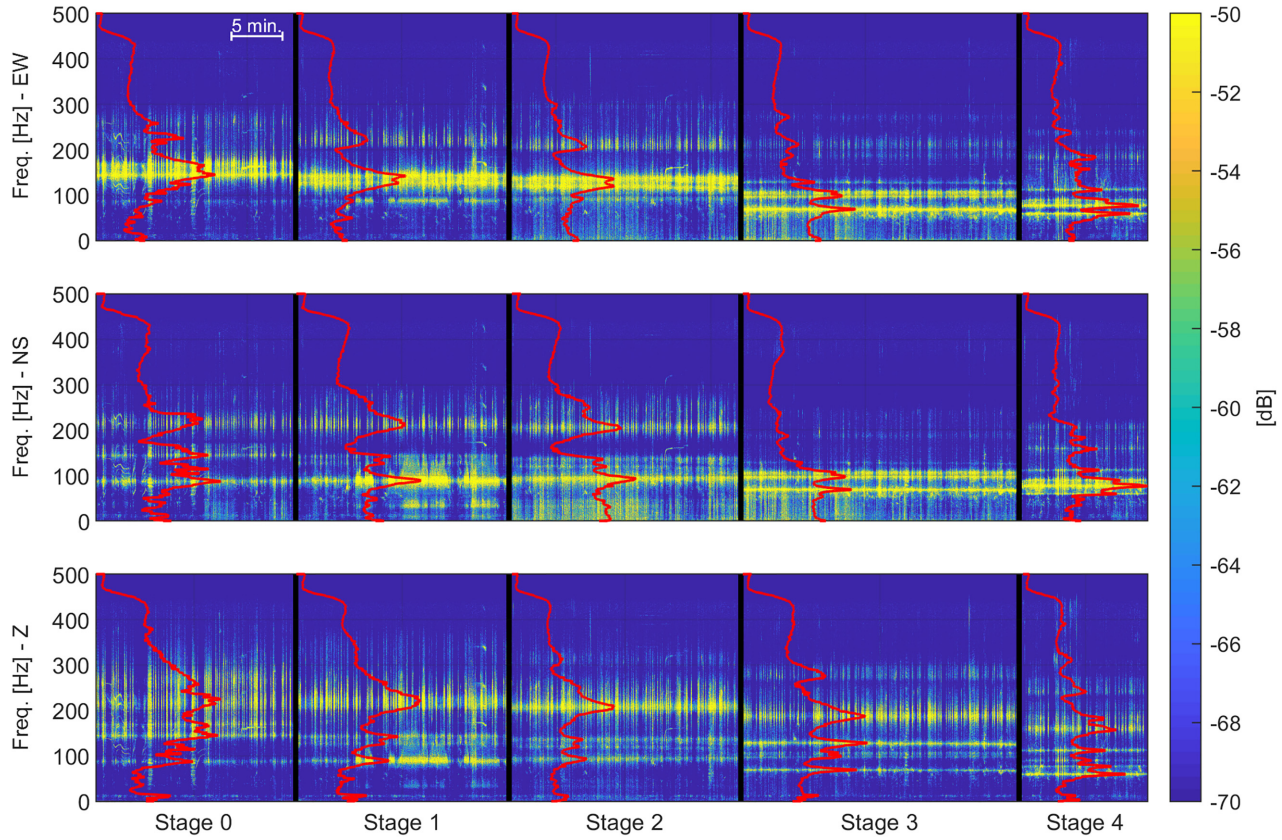

Figure 2. PSD estimates of the ambient noise recorded during the different stages of the test obtained with the MT method (red solid lines) over imposed to the spectrograms (colour map). Both the PSDs and the spectrograms are normalized to the absolute maximum of all the stages.

the spectrogram having central frequencies around 220 and 150 Hz at the initial condition (Fig. 2), we can observe a decrease roughly as large as 50 per cent before ultimate failure. The spectral plots also show that the low-frequency dominant mode has negligible energy along the NS component until the end of stage 2, while at stages 3 and, in particular, stage 4, most of the seismic energy is equally recorded by the EW and NS components. This is consistent with our expectations, because we assumed oscillation of the block mainly in the azimuthal plane and perpendicular to fracture F2 in the beginning and, as the aperture of F2 is increased and possibly affects the persistence of F1, perpendicular to both side and rear fractures towards the final stage (Fig. 1b). On the other hand, the high-frequency mode is always larger on the vertical component and has its maximum at stage 2, where its energy is comparable with the one of the low-frequency mode, before decreasing towards failure. Differently from other authors (e.g. Valentin *et al.* 2017), no significant amplifications in amplitude spectra were observed when approaching failure. In addition, causes of low-frequency signals observed during stages 2 and 3, mainly on the NS component (Fig. 2), remain unclear.

Polarization features qualitatively observed in the spectrograms are confirmed by the results obtained with the spectral SVD approach. Two general aspects can be noted by observing the plots of the polarization parameters as a function of frequency and through the following stages (Fig. 3). First, a global trend towards lower frequency can be observed, although it is very difficult to track the temporal evolution of different vibration modes because each mode presents changing energy depending upon the boundary conditions of the rock block. Second, there are broader polarization frequency bands in the beginning, that become narrower when approaching failure. We believe that the first aspect could be due to the increased size and mass of the vibrating rock block caused by the reduction of rock bridges between the rock mass and the block itself. As far as probability of the estimated parameters is concerned, we observed relatively high values at the initial stage, then a decrease across stages 1 and 2, and, finally, an increase to highest values at stage 4. This nonlinear trend of the probability values may indicate the different emergence of the vibration modes that the block experiences through the stages.

The analysis of data collected by two meteorological stations in Mandello del Lario and Abbadia Lariana shows that air temperature and wind speed experienced minor variations during the test (Fig. S2, Supporting Information), surely not sufficient to cause the observed spectral and polarization changes (Levy *et al.* 2010; Starr *et al.* 2015; Bottelin *et al.* 2017; Colombero *et al.* 2017).

Although the limited size of the investigated structure allowed for high-resolution 3-D modelling, the obtained results were unsatisfactory in terms of matching with observed data. We believe that the most critical point is to model correctly the spatial and mechanical features of the constraints. In addition, the fact that the collapse test involved two blocks separated by the bedding discontinuity may have increased uncertainty in the modelling procedure. As a consequence, we cannot infer any relationship between variations of resonance frequency versus changes in the area of rock bridges. The results of the modelling exercise we performed to match the observed resonance frequencies indicate that the frequency drop between the first and the last stages could be obtained by reducing the rock bridge area from 7.5 per cent to 2.7 per cent of the total side and

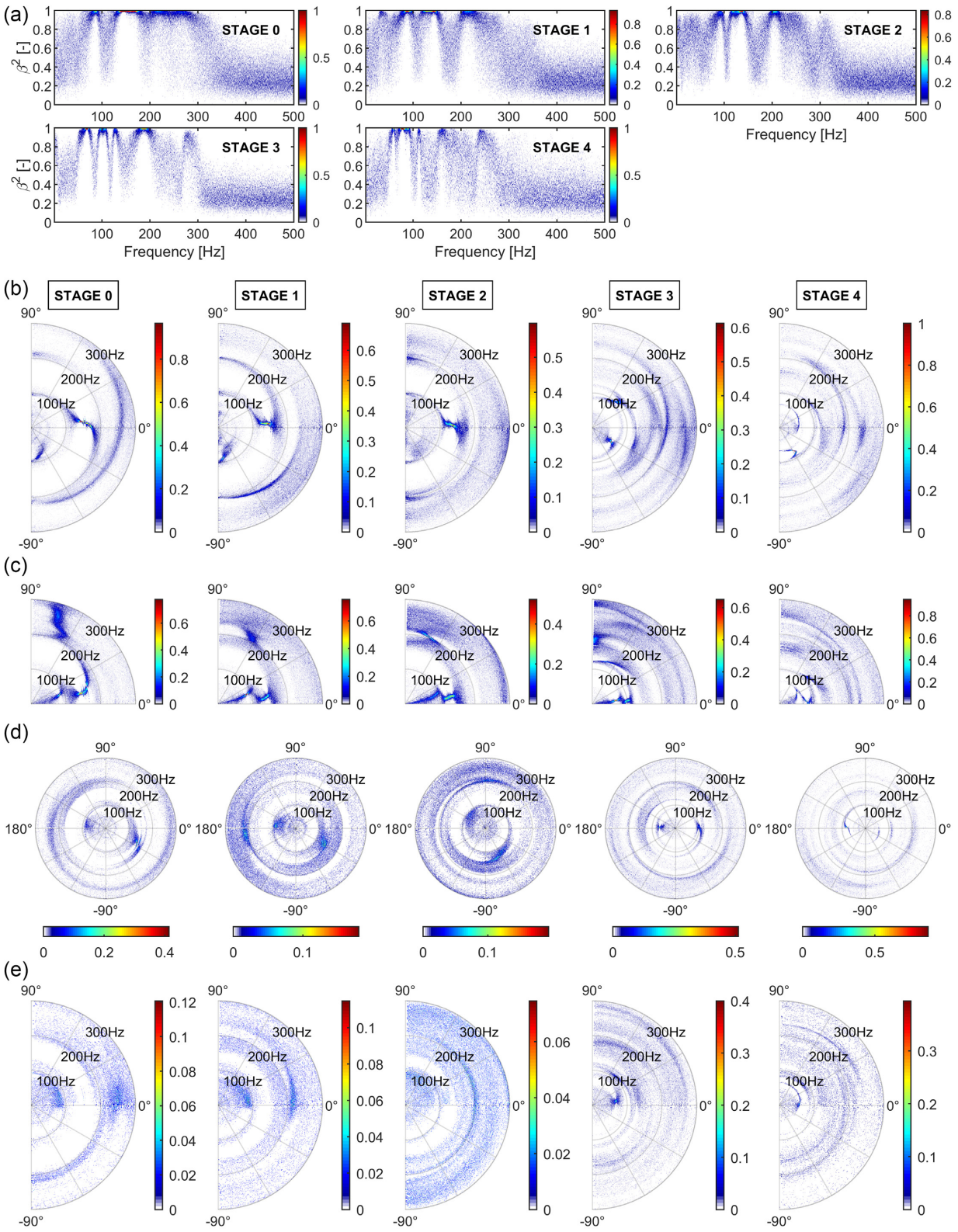

Figure 3. Polarization parameters estimated with the spectral SVD method for the different stages of the collapse test. Part (a) is the polarization degree β^2, (b) is the azimuth of the main polarization axis Θ_H, (c) is the dip measured form the horizontal of the main polarization axis Θ_V, (d) is the phase lag between the two orthogonal horizontal components ϕ_{HH} and (e) is the phase lag between the vertical and the principal horizontal components ϕ_{VH}. The colour map indicates relative probability of the estimated parameter and limits of each colour map are set to the minimum and maximum values of the related parameter. See the text for details.

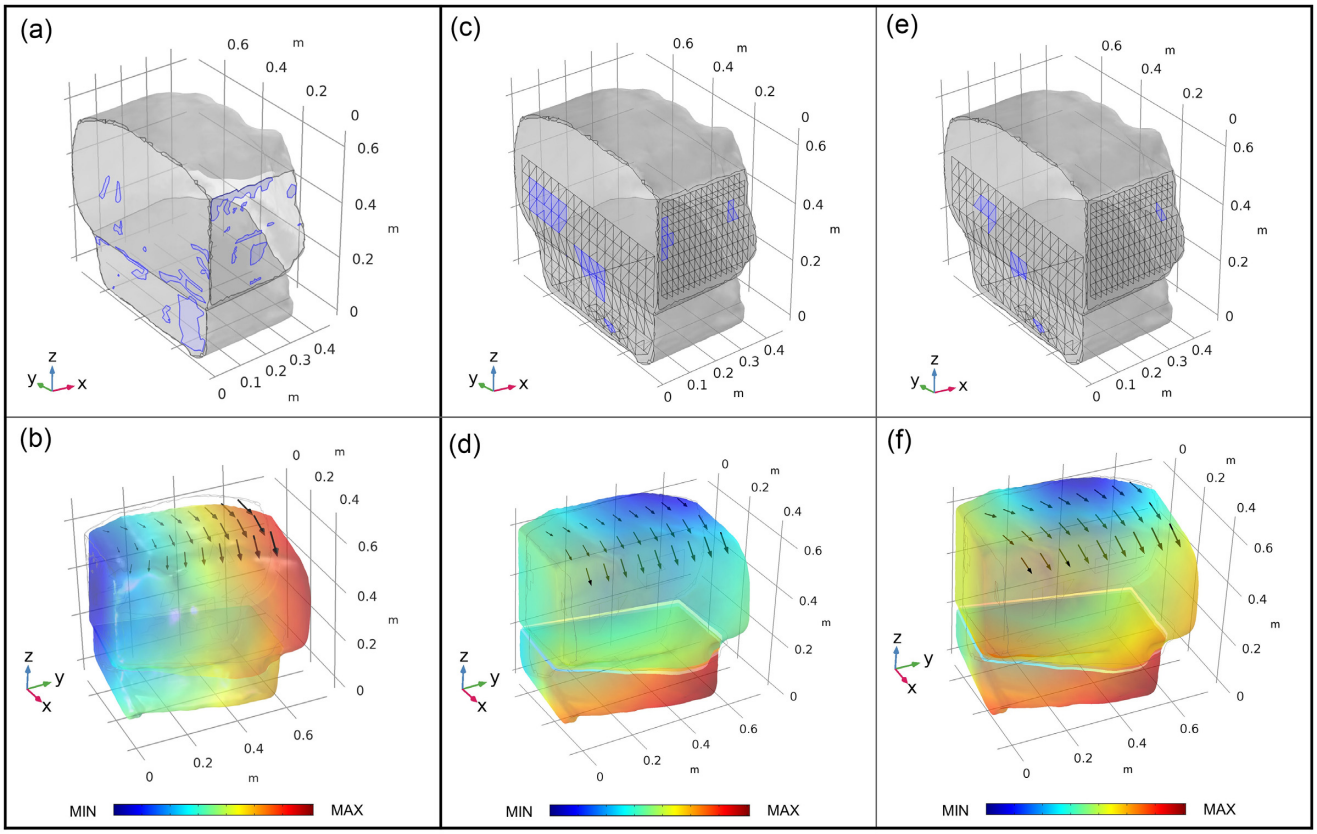

Figure 4. (a) Block model with rock bridges (in purple) estimated from the RGB matrix of near frontal images of rear and side fractures and (b) modelling results with colour map and arrows indicating displacements. (c) Block model used in the modelling exercise having discretized rear and side fractures with rock bridges (in purple) set to match the resonance frequencies observed at stage 0. (d) Modelling results for model in (c). (e) and (f) Same as (c) and (d) for stage 4.

Table 1. Resonance frequencies obtained with the SVD analysis and with the numerical modelling exercise.

	Stage 0		Stage 4	
	Polarization analysis β^2 peak (Hz)	Numerical modelling eigenfrequency (Hz)	Polarization analysis β^2 peaks (Hz)	Numerical modelling eigenfrequency (Hz)
Mode 1	87.2	86.1	59.4	56.4
Mode 2	144.6	141.7	77.1	74.3
Mode 3	168.1	185.8	89.8	97.4
Mode 4	215.1	211.5	112.2	118.5
Mode 5	260.3	265.5	160.0	158.7

rear fracture areas. This finding is in agreement with post-failure observations of fresh rupture areas performed on limestone cliffs in south-east France (Frayssines & Hantz 2006). Unfortunately, modelling was not able to reproduce modal shapes of the block in stages 0 and 4, as we observed differences nearly as large as 90° between the modelled vibration directions in the azimuthal plane and the values of Θ_H estimated with the spectral SVD method.

6 CONCLUSIONS

Failures of rock structures are sudden phenomena that pose serious threats to human settlements and infrastructures because of their difficulty to be predicted. The deployment of a microseismic monitoring network across the investigated area can provide a predictive capability based on changes of the collected waveforms, generated where the slope is mechanically unstable (Spillmann *et al.* 2007). However, several factors could reduce the performance of the sensors in detecting microseismic signals and, as a result, the effectiveness of the network as an early warning tool. Seismic noise monitoring needs no specific events to be generated since it is based on continuous recording of ambient vibrations that excite the studied rock structure and, therefore, could overcome the drawbacks of classical microseismic monitoring.

The controlled small collapse test we performed confirms previous findings according to which the collapse of an unstable rock is preceded by the drop of resonance frequencies as a consequence of the breakage of rock bridges. Spectral plots obtained from seismic noise recordings with the MT method provided evidence of the frequency decreasing trend, nevertheless, we noted that the vibration modes of the studied structure varied dynamically through the test, with some spectral peaks emerging and vanishing according to the evolving constraints of the rock block. The abrupt changes in the block vibration modes may have prevented the observation of spectral amplification phenomena. Spectral analysis of rock structures

by means of HVSR should be considered carefully because spectral division between the horizontal and vertical components may delete some frequency peaks associated to vibration modes whose vertical component dwarfs the horizontal ones. This is particularly true for rocks with arbitrary geometry and uncertain boundary conditions that, for instance, cannot be considered as a simple cantilever beam. Polarization analysis performed by means of the spectral SVD approach proved to be very useful in tracking over time the frequency bands of polarized oscillations together with their angular parameters in the 3-D space. Again, we were able to observe a shift towards lower frequencies before ultimate failure, as well as the narrowing of the polarized bands.

Generally, spectral smoothing should be applied carefully and different smoothing filters and their parameters should be tested because they may merge peaks associated to different vibration modes. Also, choice between linear and logarithmic sampling of the frequency axis should be tuned according to the bands of interest of the considered case study.

Overall, the results of our small collapse test indicate that both spectral and polarization analyses could be useful monitoring tools to track the behaviour of unstable rock compartments with arbitrary geometry over time. In fact, the spectral SVD approach alone could provide comprehensive knowledge needed for forecasting purposes. A sound monitoring approach should take into account diverse pieces of information, such as the shift, emerging and vanishing of resonance frequencies, the bandwidth of vibration modes and the changes in their polarization. Surely, the boundary conditions of the block, we forced to collapse have undergone dramatic changes in a very short period of time. This can make interpretation of the evolution of the polarization trend with frequency very complex. We believe that, in real case studies, the evolution of the dynamic conditions of a rock is not as fast, and this may allow a better tracking of the vibration modes over time. On the other hand, sudden variations of the monitored parameters may provide useful indications for early warning systems. Given the short duration of our test, we could not investigate the influence of meteorological factors on the vibration modes of the rock block. Dealing with long-term monitoring systems, one should not forget that the dynamic characteristics of the investigated structures may vary for instance as a consequence of freeze-thaw cycles or because of rock dilation/contraction linked to temperature fluctuations (e.g. Levy *et al.* 2010). Since predictive capability depends on the ability to observe subtle changes over time, the accuracy and reliability of the estimated spectral and polarization features are of fundamental importance. According to this, development of uncertainty analysis of the estimated parameters is encouraged.

Our work shows that realistic numerical modelling of the dynamic behaviour of rock structures is still a challenging task, even when considering small specimen, especially in terms of the accurate definition of the spatial and mechanical features of the constraints. Therefore, the support of modelling to guide processing and interpretation of seismic noise data still needs to be improved. However, non-destructive electromagnetic techniques, both radar and infrared, could be employed to characterize rock fractures and rock bridges in a non-destructive manner (Arosio 2016; Guerin *et al.* 2019).

ACKNOWLEDGEMENTS

We wish to thank Mary Templeton at Incorporated Research Institutions for Seismology (IRIS) for providing the nominal response for Nanometrics Trillium Compact sensor and Centaur data logger. We also thank Instrumental Software Technologies Inc. for providing Java routines to evaluate and plot sensor and logger responses. We are grateful to Daniel Pereira for making his MatLab software WindRose available to the scientific community and to Federico Gatti at Politecnico di Milano for his helpful suggestions on the MT method. Finally, we thank the Editor, Lapo Boschi, and two anonymous reviewers for their comments and suggestions that helped to improve the quality of this manuscript.

Data generated in this study are available for download at the author's website: https://drive.google.com/drive/folders/1ApmT4wqlvlCJxiNCLbZ9Djaz2JIM1i38?usp = sharing.

REFERENCES

Arosio, D., 2016. Rock fracture characterization with GPR by means of deterministic deconvolution, *J. appl. Geophys.,* **126,** 27–34.

Arosio, D., Longoni, L., Papini, M., Bièvre, G. & Zanzi, L., 2019a. Geological and geophysical investigations to analyse a lateral spreading phenomenon: the case study of Torrioni di Rialba, northern Italy, *Landslides,* **16**(7), 1257–1271.

Arosio, D., Longoni, L., Papini, M., Boccolari, M. & Zanzi, L., 2018. Analysis of microseismic signals collected on an unstable rock face in the Italian Prealps, *Geophys. J. Int.,* **213**(1), 475–488.

Arosio, D., Taruselli, M., Longoni, L., Papini, M. & Zanzi, L., 2019b. Seismic noise polarization analysis for unstable rock monitoring, in *Proceedings of the 25th European Meeting of Environmental and Engineering Geophysics, The Hague, The Netherlands,* European Association of Geoscientists & Engineers (EAGE), The Netherlands, pp. 1–5, Vol. **2019,** doi:10.3997/2214-4609.201902451.

Bottelin, P., Baillet, L., Larose, E., Jongmans, D., Hantz, D., Brenguier, O., Cadet, H. & Helmstetter, A., 2017. Monitoring rock reinforcement works with ambient vibrations: La Bourne case study (Vercors, France), *Eng. Geol.,* **226,** 136–145.

Bottelin, P. *et al.*, 2013a. Spectral analysis of prone-to-fall rock compartments using ambient vibrations, *J. Environ. Eng. Geophys.,* **18,** 205–217.

Bottelin, P., Levy, C., Baillet, L., Jongmans, D. & Gueguen, P., 2013b. Modal and thermal analysis of Les Arches unstable rock column (Vercors Massif, French Alps), *Geophys. J. Int.,* **194,** 849–858.

Burjánek, J., Gischig, V., Moore, J.R. & Fäh, D., 2018. Ambient vibration characterization and monitoring of a rock slope close to collapse, *Geophys. J. Int.,* **212,** 297–310.

Burjánek, J., Kleinbrod, U. & Fäh, D., 2019. Modelling the seismic response of unstable rock mass with deep compliant fractures, *J. geophys. Res.: Solid Earth,* **124,** 13039–13059.

Burjánek, J., Moore, J.R., Yugsi Molina, F.X. & Fäh, D., 2012. Instrumental evidence of normal mode rock slope vibration, *Geophys. J. Int.,* **188,** 559–569.

Clinton, J.F., Case Bradford, S., Heaton, T.H. & Favela, J., 2006. The observed wander of the natural frequencies in a structure, *Bull. seism. Soc. Am.,* **96**(1), 237–257.

Colombero, C., Baillet, L., Comina, C., Jongmans, D. & Vinciguerra, S., 2017. Characterization of the 3-D fracture setting of an unstable rock mass: from surface and seismic investigations to numerical modelling, *J. geophys. Res.: Solid Earth,* **122,** 6346–6366.

Del Gaudio, V. & Wasowski, J., 2007. Directivity of slope dynamic response to seismic shaking, *Geophys. Res. Lett.,* **34,** L12301.

Franklin, J.A., 1985. Suggested method for determining point load strength, *Int. J. Rock Mech. Min. Sci. Geomech. Abstr.,* **22**(2), 51–60.

Frayssines, M. & Hantz, D., 2006. Failure mechanisms and triggering factors in calcareous cliffs of the Subalpine Ranges (French Alps), *Eng. Geol.,* **86**(4), 256–270.

Guerin, A. *et al.*, 2019. Detection of rock bridges by infrared thermal imaging and modelling, *Sci. Rep.,* **9**(1), 13138.

Katz, O., Reches, Z. & Roegiers, J.C., 2000. Evaluation of mechanical rock properties using a Schmidt hammer, *Int. J. Rock. Mech. Min. Sci.,* **37,** 723–728.

Konno, K. & Ohmachi, T., 1998. Ground-motion characteristics estimated from spectral ratio between horizontal and vertical components of microtremor, *Bull. seism. Soc. Am.,* **88**(1), 228–241.

Koper, K.D. & Hawley, V.L., 2010. Frequency dependent polarization analysis of ambient seismic noise recorded at a broadband seismometer in the central United States, *Earthq. Sci.,* **23**(5), 439–447.

Kulatilake, P.H.S.W., Shreedharan, S., Sherizadeh, T., Shu, B., Xing, Y. & He, P., 2016. Laboratory estimation of rock joint stiffness and frictional parameters, *Geotech. Geol. Eng.,* **34**(6), 1723–1735.

Lévy, C., Baillet, L., Jongmans, D., Mourot, P. & Hantz, D., 2010. Dynamic response of the Chamousset rock column (Western Alps, France), *J. geophys. Res.,* **115,** F04043.

Lorenzoni, F., Caldon, M., da Porto, F., Modena, C. & Aoki, T., 2018. Post-earthquake controls and damage detection through structural health monitoring: applications in l'Aquila, *J. Civil. Struct. Health Monit.,* **8,** 217–236.

Moore, J.R., Gischig, V., Burjanek, J., Loew, S. & Fah, D., 2011. Site effects in unstable rock slopes: dynamic behavior of the Randa instability (Switzerland), *Bull. seism. Soc. Am.,* **101,** 3110–3116

Park, J., Vernon, F.L. & Lindberg, C.R., 1987. Frequency dependent polarization analysis of high-frequency seismograms, *J. geophys. Res.: Solid Earth,* **92**(B12), 12664–12674.

Percival, D.B. & Walden, A.T., 1993. *Spectral Analysis for Physical Applications: Multitaper and Conventional Univariate Techniques,* Cambridge University Press, Cambridge.

Potenza, F., Federici, F., Lepidi, M., Gattulli, V., Graziosi, F. & Colarieti, A., 2015. Long-term structural monitoring of the damaged Basilica S. Maria di Collemaggio through a low-cost wireless sensor network, *J. Civil. Struct. Health Monit.,* **5,** 655–676.

Saisi, A., Gentile, C. & Guidobaldi, M., 2015. Post-earthquake continuous dynamic monitoring of the Gabbia Tower in Mantua, Italy, *Constr. Build. Mater.,* **81,** 101–112.

Samson, J.C., 1983. Pure states, polarized waves, and principal components in the spectra of multiple, geophysical time-series, *Geophys. J. R. astr. Soc.,* **72,** 647–664.

Spillmann, T., Maurer, H., Green, A.G., Heincke, B., Willenberg, H. & Husen, S., 2007. Microseismic investigation of an unstable mountain slope in the Swiss Alps, *J. geophys. Res.: Solid Earth,* **112,** B07301.

Sonmez, H., Gokceoglu, C., Nefeslioglu, H.A. & Kayabasi, A., 2006. Estimation of rock modulus: for intact rocks with an artificial neural network and for rock masses with a new empirical equation, *Int. J. Rock Mech. Min. Sci.,* **43**(2), 224–235.

Starr, A.M., Moore, J.R. & Thorne, M.S., 2015. Ambient resonance of Mesa Arch, Canyonlands National Park, Utah, *Geophys. Res. Lett.,* **42,** 6696–6702.

Templeton, M.E., 2017. *IRIS Library of Nominal Response for Seismic Instruments. Incorporated Research Institutions for Seismology*. Dataset. doi:10.17611/S7159Q.

Thomson, D.J., 1982. Spectrum estimation and harmonic analysis, *Proc. IEEE,* **70,** 1055–1096.

Valentin, J., Capron, A., Jongmans, D., Baillet, L., Bottelin, P., Donze, F., Larose, E. & Mangeney, A., 2017. The dynamic response of prone-to-fall columns to ambient vibrations: comparison between measurements and numerical modelling, *Geophys. J. Int.,* **208**(2), 1058–1076.

SUPPORTING INFORMATION

Supplementary data are available at *GJI* online.

Figure S1. Control points used to monitor the aperture of fracture F2 during the collapse test. Fracture aperture was measured with a digital calliper.

Figure S2. Meteorological data collected by the climatic stations installed close to the Como Lake in Abbadia Lariana and in Mandello del Lario, roughly 5.5 and 4 km south of the test site, respectively. (a) Air temperature (vertical grey lines mark the beginning of each stage of the test). Polar plot of wind speed measured in (b) Abbadia Lariana and in (c) Mandello del Lario.

Figure S3. Polarization parameters estimated with the spectral SVD method for stages (a) 0, (b) 1, (c) 2, (d) 3 and (e) 4 of the collapse test. The colour map indicates relative probability of the estimated parameter and limits of each colour map are set to the minimum and maximum values of the related parameter. See the text of the manuscript for details.

Please note: Oxford University Press is not responsible for the content or functionality of any supporting materials supplied by the authors. Any queries (other than missing material) should be directed to the corresponding author for the paper.